*Defect and Diffusion Forum Vols. 237-240 (2005) pp. 1016-1021*
*online at http://www.scientific.net*


# Impedance Spectroscopy Study of Li Ion Dynamics in Single Crystal, Microcrystalline, Nanocrystalline, and Amorphous $LiNbO_3$

Muayad Masoud and Paul Heitjans

Institut für Physikalische Chemie und Elektrochemie, Universität Hannover, Callinstr. 3-3a, 30167 Hannover, Germany

heitjans@pci.uni-hannover.de

**Keywords:** Lithium niobate, nanocrystalline ceramics, amorphous, lithium diffusion, impedance spectroscopy, conductivity.

**Abstract.** Impedance spectroscopy was employed to investigate the Li ion diffusivity in single crystal, microcrystalline, nanocrystalline and amorphous lithium niobate ($LiNbO_3$). Nanocrystalline $LiNbO_3$ with different grain sizes was prepared by high-energy ball milling from the microcrystalline starting material. The amorphous form was prepared by a double alkoxide (sol-gel) route. The frequency dependent conductivity was measured under oxygen atmosphere at frequencies, $\omega/2\pi$, ranging from 5 Hz to 13 MHz. The ionic conductivity at, e.g., 450 K was found to increase by about seven orders of magnitude by going from the single crystal through the microcrystalline to the corresponding nanocrystalline and amorphous forms. The increased free volume in the amorphous material could be responsible for the enhanced conductivity, whereas in nanocrystalline $LiNbO_3$ the behavior is governed by the increased fraction of the interfacial regions which are highly disordered and may in the present case be visualized as amorphous. In all cases the frequency dependence of the real part of the conductivity can be represented by a power law and can be scaled to give master curves. Impedance data were analyzed in the complex plane plot (with $\omega$ as implicit parameter). Both the dc conductivity and the relaxation frequency of the impedance arc, $\omega_r/2\pi$, were found to follow Arrhenius behaviour with similar activation energies.

## Introduction

Lithium niobate is a well-known ferroelectric human-made oxide material that has attracted a great deal of interest for both basic science and technology. Due to the unusual richness in its physical properties, during the last three decades it was the subject of a large number of papers, reviews and even books [1-3]. In many of its applications various diffusion processes are important for the production of the required material with tailored properties [4].

Li-ion containing ceramics have been of great interest as solid-state electrolytes with several potential applications, mainly in primary and secondary batteries. In general, the diffusivity of Li ions was found to increase when going over from the microcrystalline form to the corresponding (i) nanocrystalline [5] or (ii) amorphous forms [6], or (iii) by admixture of a nanocrystalline ionic insulator to a nanocrystalline ionic conductor [7]. In cases (i) and (iii) the increased volume fraction of the grain boundaries or interfacial regions, respectively, is most likely to be responsible for the faster atomic transport. These regions are highly disordered or defective and tolerate the excess free energy attained during the preparation. Contrarily, ion movement inside the grains is limited. In case (ii) the "free volume" in the network has been used to explain the fast diffusion of ions. Accordingly, it was previously found in our group, by means of a NMR study, that the Li diffusivity is increased drastically in nanocrystalline $LiNbO_3$ compared with the microcrystalline form [8]. Li diffusion in amorphous $LiNbO_3$ was described by the same diffusion parameters as in nanocrystalline form [9].

The majority of the extensive work done on $LiNbO_3$ was aimed at $LiNbO_3$ single crystals [10-14]. The piezoelectric behavior was probed in polycrystalline $LiNbO_3$ ceramics [15] as well as its conductivity and dielectric constant [16]. Glass et al. [17] and Nassau [18] were the first to prepare amorphous $LiNbO_3$ by twin roller quenching and to investigate its electrical properties. Later Kim et al. [19] investigated its thermal and electrical properties.

In the present study we enclose all the previous forms of $LiNbO_3$ in addition to nanocrystalline $LiNbO_3$ prepared by high-energy ball milling (H.E.B.M.) with different grain sizes, and the amorphous form prepared by a sol-gel route.

Impedance spectroscopy (IS) is a widely recognized powerful tool for investigating the electrical behaviour of ionic, electronic or mixed conducting ceramics [20]. In IS, the current amplitude and phase angle are measured in response to an applied alternating voltage at frequencies, $f = \omega/2\pi$, ranging from less than one Hz to some tens of MHz.

The impedance of the sample, $Z^* = Z' - iZ''$, is well represented by the complex plane diagram. The negative of the imaginary part of the impedance, $-Z''$, is plotted vs. the real part, $Z'$. This representation enables a separation of the different processes in ionically conducting samples. In the ideal case, nanocrystalline samples are expected to show three semicircles due to the contacts (electrodes), the grain boundaries, and bulk (grain) conductivity. Each semicircle is represented by a capacitor connected in parallel to a resistor. These $RC$ circuits are connected in series.

For relatively low-conductive materials, it is more common to deal with the reciprocal of the impedance, the admittance $Y^* = G + iB$, where $G$ is the conductance and $B$ is the susceptance. Usually conductivity is plotted as the real part of the complex admittance, $\sigma' = G \cdot l / a$, versus frequency, $f$, in a log-log plot, where $l$ and $a$ are the thickness and the area of the sample, respectively. The frequency dependent conductivity data have often been described by the empirical relation

$$\sigma' = \sigma_{dc} + A\omega^s \tag{1}$$

where $\sigma_{dc}$ is the frequency independent dc conductivity and $s$ is a temperature dependent exponent which lies between 0 and 1. $\sigma_{dc}$ is thermally activated and follows the Arrhenius relation

$$\sigma_{dc} = A' \exp(-E_{a,\sigma} / k_B T) \tag{2}$$

Here, $E_{a,\sigma}$ is the dc activation energy, $A'$ is the pre-exponential factor, $k_B$ is the Boltzmann constant and $T$ is the absolute temperature. The so-called conductivity relaxation frequency, $f_r$, can be derived for the sample equivalent circuit with resistance $R$ and capacitance $C$ from the equation

$$f_r = 1 / (2\pi RC) \tag{3}$$

The temperature dependence of $f_r$ usually follows the Arrhenius relation

$$f_r = \exp(-E_{a,r} / k_B T) \tag{4}$$

where $E_{a,r}$ is the activation energy of $f_r$ and $f_0$ is the pre-exponential factor.

**Experimental**

Highly pure (99.9995%) coarse-grained mirocrystalline $LiNbO_3$ was obtained from Alpha Aesar. Nanocrystalline ceramics were prepared from the microcrystalline powder by high-energy ball milling using a Spex 8000 mill equipped with an alumina vial. The average grain size was varied by milling for different durations of time. The average grain size of the nanocrystalline $LiNbO_3$ was determined from the line broadening of the XRD lines using the Scherrer equation [21]. The average crystallite size obtained after milling for 16 h was about 20 nm (for more details see [22]).

Amorphous $LiNbO_3$ was prepared by a sol-gel route through complete hydrolysis of lithium niobium double alkoxide followed by calcination at 470 K for two hours, as described in [23]. The XRD pattern of the sol-gel prepared sample confirmed its amorphous nature, while a sol-gel sample, re-crystallized at 570 K, gave the well-defined characteristic pattern of crystalline $LiNbO_3$.

The $LiNbO_3$ single crystal, delivered by MaTecK (Jülich, Germany), was characterized by the x-ray Guinier method. Rietveld refinement gave cell parameters $a = 5.15289$ Å and $c = 13.87161$ Å. Differential thermal analysis (DTA) of the nanocrystalline $LiNbO_3$ showed a characteristic broad exothermic peak indicating grain growth above 500 K. Therefore, the measurements for the nanocrystalline as well as for the amorphous samples were restricted to temperatures below 450 K. Microcrystalline and single crystal $LiNbO_3$ has a high thermal stability up to more than 1270 K.

Samples for impedance measurements were prepared from the corresponding powders by pressing into pellets under uniaxial pressure of 0.75 GPa. The thickness of the pellets was in the range 0.2 – 0.4 mm. The $LiNbO_3$ single crystal was cut into plates with a thickness of 0.45 mm and an area of 15 × 12 $mm^2$. The two largest parallel surfaces were polished and sputtered with gold.

The conductivity measurements were performed using a glass cell placed in a horizontal-tube furnace. The temperature was changed in 10-degrees steps. Impedance spectra were measured in the frequency range 5 Hz – 13 MHz using an HP 4192A impedance analyzer with impedance detection range 0.1 mΩ – 1 MΩ. Because of the low conductivity of the single crystal, in this case an Alpha high-resolution dielectric analyzer (Novocontrol) was used which is working in the frequency range 3 μHz - 10 MHz and in the impedance range $10^{-2}$ to $10^{14}$ Ω.

**Results and Discussion**

Fig. 1 shows typical log-log conductivity curves for amorphous $LiNbO_3$ at temperatures in the range 310 - 450 K. The curves consist of well-defined $\sigma_{dc}$-plateaus at low frequencies and a dispersive regime in the high-frequency range. The frequency dependent conductivity data were found to obey a power law, Eq. 1, with $0.55 < s < 0.77$. The decrease of $\sigma'$ for $f < 10$ Hz, visible in the high-temperature conductivity curves, is due to blocking electrode effects. With increasing temperature, the onset frequency of the dispersive range shifts towards higher frequencies following a straight line with slope of about 1. Sliding the conductivity isotherms for amorphous $LiNbO_3$ along this line makes them to collapse into a common curve. This can be achieved by scaling the $y$-axis with $\sigma_{dc}$ and the $x$-axis with $(\sigma_{dc} \cdot T)$ implying that the underlying transport processes become faster with increasing temperature without any alteration in the conduction mechanism [25]. Fig. 2 displays the master curves for different forms of $LiNbO_3$. The curve (a) for amorphous $LiNbO_3$ coincides with those for the nanocrystalline samples after 64 h and 48 h H.E.B.M., while the 16 h H.E.B.M. curve (b) deviates toward the curve (c) for the microcrystalline form which is shifted towards higher $(f/\sigma_{dc} \cdot T)$. The single crystal curve (d) exhibits an extra shift. At a given $(f/\sigma_{dc} \cdot T)$ value ('normalized frequency'), the normalized conductivity increases by going from single crystal $LiNbO_3$ to the microcrystalline passing through the nanocrystalline forms and ending with the amorphous material. There may be two reasons for this behaviour. (i) One reason may

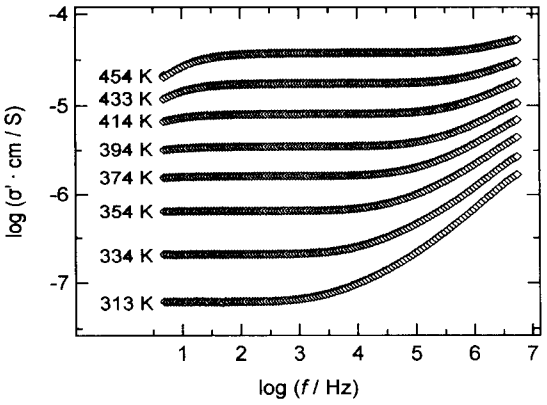


Fig. 1: Conductivity log-log curves for amorphous $LiNbO_3$ for various temperatures.

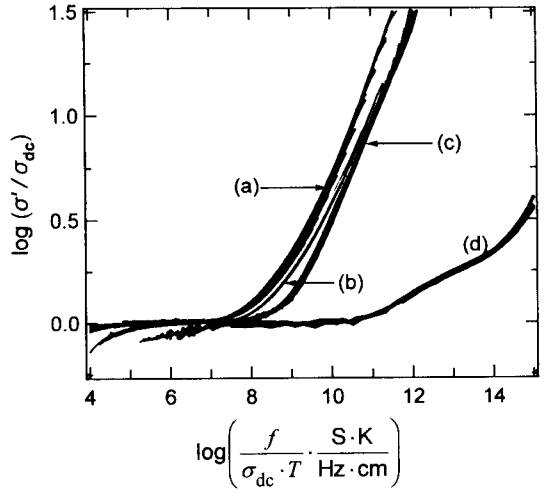


Fig. 2: Conductivity master curves for (a) amorphous and nano 64 h, 48 h; (b) nano 16 h; (c) microcrystalline; (d) single crystal $LiNbO_3$.

be the increased number of highly mobile ions due to the interfacial regions and the free volume in the nanocrystalline and amorphous forms, respectively. (ii) Alternatively one may conceive that in the amorphous material and in the interfacial regions of the nanocrystalline material the disorder leads to a lack of Brillouin zones and selection rules causing the vibrations to dominate the ionic movement [24].

Fig. 3 shows Arrhenius plots for the different forms of $LiNbO_3$. The activation energy, obtained from Eq. 2, decreases from that for single crystal and microcrystalline via nanocrystalline to that for amorphous $LiNbO_3$. Note that the activation energies of the amorphous and nanocrystalline forms are similar (Table 1).

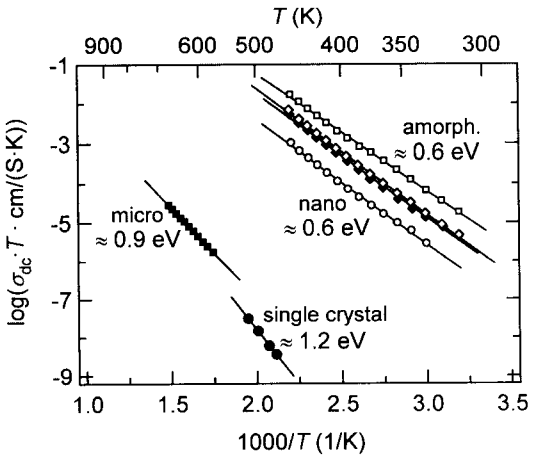


Fig. 3: Temperature dependence of $\sigma_{dc}$ for single crystal (●), microcrystalline (■), nanocrystalline [16 h (○), 48 h (♦), 64 h (◊)] and amorphous (□) $LiNbO_3$.

Table 1: Comparison between the activation energy of the dc conductivity, $E_{a,\sigma}$, and the activation energy of the semicircle relaxation frequency, $E_{a,r}$.

| $LiNbO_3$ | | $E_{a,\sigma}$ [eV] | $E_{a,r}$ [eV] |
|---|---|---|---|
| Single crystal | | 1.16 | - |
| Microcrystalline | | 0.93 | 0.88 |
| Nanocrystalline | 16 h | 0.63 | 0.58 |
| | 48 h | 0.63 | 0.59 |
| | 64 h | 0.63 | 0.60 |
| Amorphous | | 0.59 | 0.60 |

The complex impedance analysis was used to separate $\sigma_{dc}$ of the sample from electrode effects. Here the complex resistivity, $\rho^* = Z^* \cdot a/l$, is used to eliminate any differences due to the geometries of the different samples. The complex plane plots of the resistivity for different forms of $LiNbO_3$ at 370 K are shown in Fig. 4. The semicircle in each case represents the sample response, in addition to a well-behaved low-frequency inclined spike which is attributed to polarization of electrodes. These plots were analyzed using equivalent circuit software [26]. The equivalent circuit, shown in Fig. 4 (inset), represents electric and dielectric properties of $LiNbO_3$ samples. A resistor, $R_S$, and a constant phase element, $Q_S$, connected in parallel, are used to represent the response of the sample. This sub-circuit is connected in series with another constant phase element, $Q_e$, which represents the electrode response. The parameters $Q_S$ and $Q_e$ are non-ideal capacitances which allow for a distribution of relaxation times. They are physically determined by the parameters $Y_0$ and $n$ ($n \leq 1$), where $Y_0$ is the admittance of the constant phase element at angular frequency $\omega = 1$ rad/s and $n$ is the power of the constant phase element. To calculate the equivalent values for the ideal capacitor, $C$, the values of $R$, $Y_0$, $n$, obtained from the complex plane fitting, can be inserted into the relation

$$C = R^{(1-n)/n} Y_0^{1/n}. \tag{5}$$

The sample relaxation frequency, $f_r$, for different temperatures is obtained by substituting the values of $R$ and $C$ in Eq. 3. The relaxation frequencies are thermally activated according to Eq. 4, and the resultant activation energies, $E_{a,r}$, are comparable to those for $\sigma_{dc}$ (cf. Table 1). The advantage in using the relaxation frequency is its complete independence of the sample dimension.

Nanocrystalline $LiNbO_3$ shows only one depressed semicircle for both the grain interior and boundary. This might be explained by (i) the fact that the grain boundary semicircle is absent (highly conductive grain boundary), (ii) the time constants for both processes are identical, or alternatively,

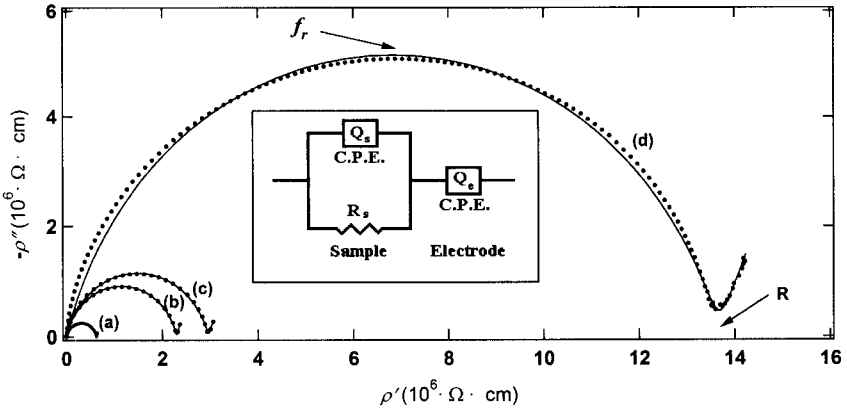


Fig. 4: Complex plane representation of the resistivity data (dotted lines) for $LiNbO_3$ at 370 K: (a) amorphous, (b) nano 64 h, (c) nano 48 h, (d) nano 16 h. The solid lines indicate the theoretical fittings obtained by an equivalent circuit program with the equivalent circuit, $(R_S Q_S)Q_e$, shown in the inset.

(iii) the grain interior contribution is too small to be detectable [27]. In our case, the second explanation is more probable suggesting that the depressed semicircle is composed of two indistinguishable semicircles with very similar relaxation times. The impedance semicircles overlap significantly if their relaxation times differ by less than three orders of magnitude [28]. There is a high degree of similarity between amorphous and nanocrystalline $LiNbO_3$ in the values of both $E_{a,\sigma}$ and $E_{a,r}$ (Table 1), in addition to the coincidence of their master curves, mainly in the case of the nanocrystalline samples milled for 48 h and 64 h (Fig. 2). This implies that the disorder in the amorphous material and the interfacial regions of the nanocrystalline one can be visualized to have similar nature. The minor differences between them, mainly in the values of conductivity, can be due to the difference in their chemical origin, and in the volume fraction of the disordered region which increases in the nanocrystalline materials with increasing milling time, whereas the amorphous form can be regarded as homogeneously disordered.

**Comparison with Previous Results**

Regarding results from the literature, the electrical conductivity was intensively investigated for pure and doped single crystal $LiNbO_3$. According to the dominant conduction mechanism, the conductivity has been categorized into three main regions [1,3]: (i) At temperatures below 400 K the conductivity is assumed to result from random hopping of electrons [29]. The activation energies for $\sigma_{dc}$ in this region are usually measured by indirect methods. (ii) In the range 400 to 1000 K there is a kind of agreement that the conduction is extrinsic and due to mobile protons diffusing in the form of $OH^-$. The activation energies range from 1.0 to 1.5 eV [11,13,30-31]. Our value of 1.2 eV (Fig. 3) agrees with the literature values. (iii) The intrinsic conduction starts at temperatures higher than 1000 K, where the conductivity depends on the oxygen partial pressure, $\sigma \propto p_{O_2}^{1/4}$, with electrons being the main charge carriers for $p_{O_2} < 1$ atm, whereas for $p_{O_2} > 1$ atm the ionic conductivity dominates the electrical response. This was explained by singly ionized oxygen vacancies. At constant $p_{O_2}$ the activation energy $E_{a,\sigma}$ was found to vary between 2.0 and 2.5 eV [14,30,32]. Lanfredi et al. [16] prepared microcrystalline $LiNbO_3$ by a chemical evaporation method followed by calcination at 820 K which showed $E_{a,\sigma} = 1.15$ eV in the temperature range 720-1070 K.

To our knowledge, in the present work the first conductivity measurements were done on nanocrystalline $LiNbO_3$. However, amorphous $LiNbO_3$ was previously prepared by several methods; early attempts were by twin-roller quenching and gave $E_{a,\sigma} = 0.4$ eV [17], Kim et al. [19] found a value of 0.50 eV for their sample prepared by the same method. Ono et al. [22] prepared amorphous

$LiNbO_3$ by a sol gel method using the same chemical route as applied here and found $E_{a,\sigma} = 0.47$ eV.

## Conclusion

Li ion motion is relatively slow in crystalline $LiNbO_3$ unless a higher degree of disorder is introduced in the Li sublattice. This can be accomplished by ball milling by which the parent microcrystalline material is converted into nanocrystals with highly defective interfacial regions. It is also achieved in amorphous materials due to "free volume" enclosed in its disordered network. Following this concept, the ionic conductivity was found to increase by several orders of magnitude, going from single crystal via microcrystalline to nanocrystalline and amorphous $LiNbO_3$. The activation energy of conductivity decreases along the same lines. The high resemblance of conductivity behaviour implies that the disorder in the amorphous material and in the interfacial regions of the nanocrystalline $LiNbO_3$ prepared by ball milling can be visualized to have similar nature.

## Acknowledgements

The authors wish to express their sincere appreciation to C. Rüscher, H. Behrens and T. Gesing from Institut für Mineralogie, Universität Hannover, for their help and technical support. We also like to thank M. Klüppel, J. Meier and B. Hünke from Deutsches Institut für Kautschuktechnologie for technical support. M. M. would like to acknowledge a grant of the graduate program "New Materials with Tailored Properties" of the Zentrum für Festkörperchemie und Neue Materialien (ZFM), Universität Hannover.

## References

[1] K. Wong (Ed.): *Properties of Lithium Niobate*, (INSPEC, UK, 2002).
[2] R. Weis and T. Gaylord: Appl. Phys. A **37** (1985) 191.
[3] A. Räuber, in *Current Topic Materials Science*, ed. by E. Kaldis, (North-Holland, Amsterdam, 1978) p.481
[4] D. Birnie III: J. Mater. Sci. **28** (1993) 302.
[5] P. Heitjans and S. Indris: J. Phys.: Condens. Matter **15** (2003) R1257.
[6] R. Winter, K. Siegmund and P. Heitjans: J. Non-Cryst. Solids **212** (1997) 215.
[7] S. Indris, P. Heitjans, H. Roman and A. Bunde: Phys. Rev. Lett. **84** (2000) 2889.
[8] D. Bork and P. Heitjans: J. Phys. Chem. B **105** (2001) 9162.
[9] M. Wilkening, D. Bork, S. Indris and P. Heitjans: Phys. Chem. Chem. Phys. **4** (2002) 3246.
[10] Z. Shapiro, S. Fedulov, Y. Venevtse and L. Rigerman: Sov. Phys. Crystallogr. **10** (1966) 725.
[11] W. Bollmann and M. Gernand: Phys. Status Solidi A **9** (1972) p. 301
[12] V. Antonov, P. Arsenev, B. Baranov, A. Mayer and V. Farshten: Phys. Status Solidi A **17** (1973) K61.
[13] S. Kaul and K. Singh: Solid State Comun. **26** (1978) 365.
[14] P. Jorgensen and R. Bartlett: J. Phys. Chem. Solids **30** (1969) 2639.
[15] Y. Xi, H. Mckinstry and L. Cross: J. Amer. Ceram. Soc. **66** (1983) 637.
[16] S. Lanfredi and A. Rodrigues: J. Appl. Phys. **86** (1999) 2215.
[17] A. Glass, K. Nassau and T. Negran: J. Appl. Phys. **49** (1978) 4808.
[18] K. Nassau: J. Non-Cryst. Solids **42** (1980) 423.
[19] S. Kim, M Jang, B Chae and Y Yang: J. Korean Phys. Soc. **32** (1998) S807.
[20] J. R. Macdonald (Ed.), *Impedance Spectroscopy*, (Wiley, New York, 1987).
[21] H. P. Klug and L. E. Alexander, *X-ray Diffraction Procedures*, (Wiley, New York, 1974).
[22] S. Indris, D. Bork and P. Heitjans: J. Mater. Synth. Proc. **8** (2000) 245.
[23] S. Ono, H. Mochizuki and S. Hirano J. Cer. Soc. Jap. **104** (1996) 574.
[24] K. Funke, C. Cramer and B. Roling: Glass. Sci. Technol. **73** (2000) 244.
[25] S. Summerfield: Philos. Mag. B **52** (1985) 9.
[26] B. Boukamp, *Equivalent Circuit, Version 4.51*, (University of Twente, Netherlands, 1993).
[27] J. Lee, J. Hwang, J. Mashek, T. Mason, A. Miller and R. Siegel: J. Mater. Res. **10** (1995) 2295.
[28] M. Kleitz and J. Kennedy, in *Fast Ion Transport in Solids: Electrodes and Electrolytes*, ed. by P. Vashishta, J. Mundy and G. Shenoy, (North-Holland, Amsterdam, 1979) p.185
[29] A. Mansingh and A. Dhar: J. Phys. D: Appl. Phys. **18** (1985) 2059.
[30] G. Bergmann: Solid State Commun. **6** (1968) 77.
[31] L. Kovacs, I. Fodvari and K. Polgar: Acta Phys. Hung. **61** (1987) 223.
[32] Y. Limb; K. Cheng and D. Smyth: Ferroelectrics **38** (1981) 813.